TIDAL CURRENTS AND SAND BAR EVOLUTION IN SITTAUNG RIVER ESTUARY, MYANMAR

TANJIR SAIF AHMED
International Center for Water Hazard and Risk Management, Public Works Research Institute, Minamihara 1-6, Tsukuba, Ibaraki, Japan, s-tanjir@icharm.org

SHINJI EGASHIRA
International Center for Water Hazard and Risk Management, Public Works Research Institute, Minamihara 1-6, Tsukuba, Ibaraki, Japan, s-egashira77@pwri.go.jp

DAISUKE HARADA
International Center for Water Hazard and Risk Management, Public Works Research Institute, Minamihara 1-6, Tsukuba, Ibaraki, Japan, d-harada55@pwri.go.jp

ABSTRACT

The Sittaung river estuary is 220 km long southwards and 270 km wide and it opens to Gulf of Martaban. Due to a funnel shape of the estuary, tidal bores and associated strong currents take place during spring tides on new moon and full moon. Bed and banks of the estuary are constituted by silt and clay particles with their d_{50} ranging from 0.02 to 0.04 mm. Therefore, a very active sediment transportation takes place with active channel changes leading to severe bank erosion at the rate of around 1 km every year at most active locations. Present study discusses tidal currents and associated channel changes with sand bar evolution based on numerical results obtained from a newly proposed model. The new model is composed of a sediment transport process model to treat very fine sediment such as silt-clay material in addition to a depth-averaged two dimensional flow model. Numerical results show that tidal bores and associated strong currents are reproduced well. Bed evolution and channel pattern are reproduced for the shape of estuary in recent years. Numerically created morphology agrees well with the recent satellite images extracted during ebb tides.

Keywords: Estuary, numerical model, fine sediment, sand bar deformation, channel changes.

1. INTRODUCTION

Figure 1 shows a place of Sittaung river and associated sites. The river stretches northward from the mouth and it drains the area of about 36000 km^2 at the Sittaung Bridge. The estuary spreads towards south from the Sittaung Bridge with a funnel shape and is open to Gulf of Martaban. Because of this shape, tidal bores and associated strong currents take place in early spring and early autumn, resulting in movement of sand bars and bank line retreat. Such geomorphic changes have been discussed using numerical models (e.g. Lanzoni and Seminara, 2002; Lesser et al., 2004; Yu et al., 2012). Shimozono et al. (2019) studied morphological changes in the present study area and identified an auto-cyclic process in a sedimentary system driving large scale channel migration in decadal to multi-decadal cycles. In addition, they discussed evolution of the estuary on different time scales, cyclic channel migration sub-processes based on Landsat image analysis. Robinson et al. (2007) estimated sediment flux of Irrawaddy as high as 364 ± 60 MT yr^{-1}, Irrawaddy-Salween system as 370-600 MT yr^{-1} and concluded Irrawaddy as third-largest contributor of sediment load after the Amazon and Ganges-Brahmaputra. Ramaswamy et al. (2004) suggested that the sea floor of the Gulf of Martaban, the surrounding coastal areas and estuaries are covered with silty clays and a major portion of the

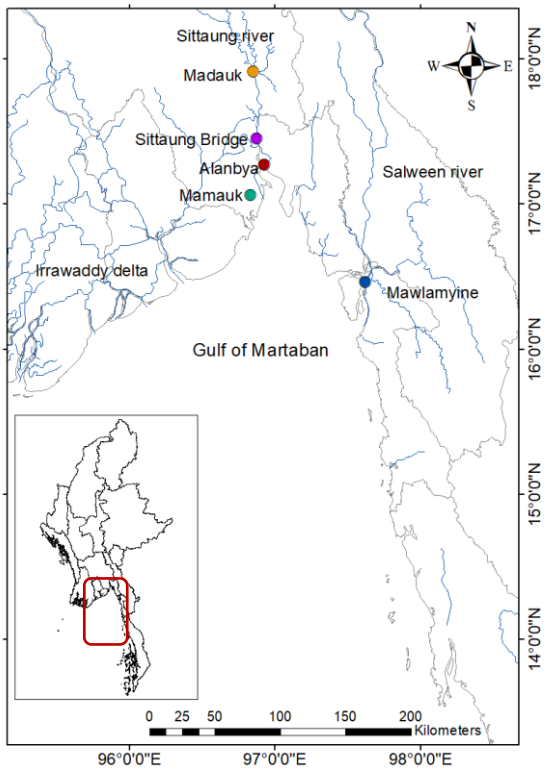

Figure 1. Sittaung river estuary region.

suspended material must be derived from resuspension of these sediments. They propose that a huge sediment load incoming from Irrawaddy-Salween system is re-suspended by the strong tidal currents and transported and distributed in the Sittaung estuary region.

We conducted field investigation on February in 2017, 2018 and 2019 to observe propagation of tidal bore, associated strong tidal currents, sediment transport characteristics and bank erosion at several locations along the west bank line near Mamauk which have been severely affected in recent years. Ahmed et al. (2019) discussed characteristics of a part of Sittaung estuary based on the field data as well as on numerical results of tidal currents and associated sediment transportation with active channel changes. In the present study, characteristics of Sittaung estuary and numerical model are shown briefly. Then, we discuss tidal bores, tidal currents, sediment transportation and associated channel changes based on numerical results as well as on satellite images.

2. CHARACTERISTIC OF STUDY AREA

Figure 2 shows Landsat 8 composite satellite image on January 14, 2020. Locations of Sittuang Bridge which is around 10 km upstream of the mouth of estuary, Alanbya village and Mamauk are also illustrated. Bank lines during January, 2015 and April, 2017 extracted from Landsat composite raster images are superimposed on recent image on January, 2020. It is clearly identified that very severe bank line retreat was occurred in recent years and Mamauk already disappeared due to bank line shifting.

Figure 3 shows sediment size distribution of representative samples of bed and bank materials collected at different locations during the field investigation in 2019. Bed materials are collected up to 25 km upstream of the Sittaung Bridge and the bank materials are collected near Mamauk. The sediment size curves suggest that sediment particles ranging 0.1 to 1.0 mm exist along the channel reach in the upstream of the Bridge, although coarser material than 0.1 mm is found rarely in the estuary bed. It is realized that grain sizes of the estuary bed are same as those collected in the river and estuary banks, and that bed material in the lower river reach and estuary is supplied from bank regions owing to erosion (Ahmed et al., 2019). Tides are measured by University of Hawaii Sea Level Center (UHSLC) at Mawlamyine which shows that tidal range varies from less than 2 m to more than 4 m fortnightly. Figure 4 shows observed data by

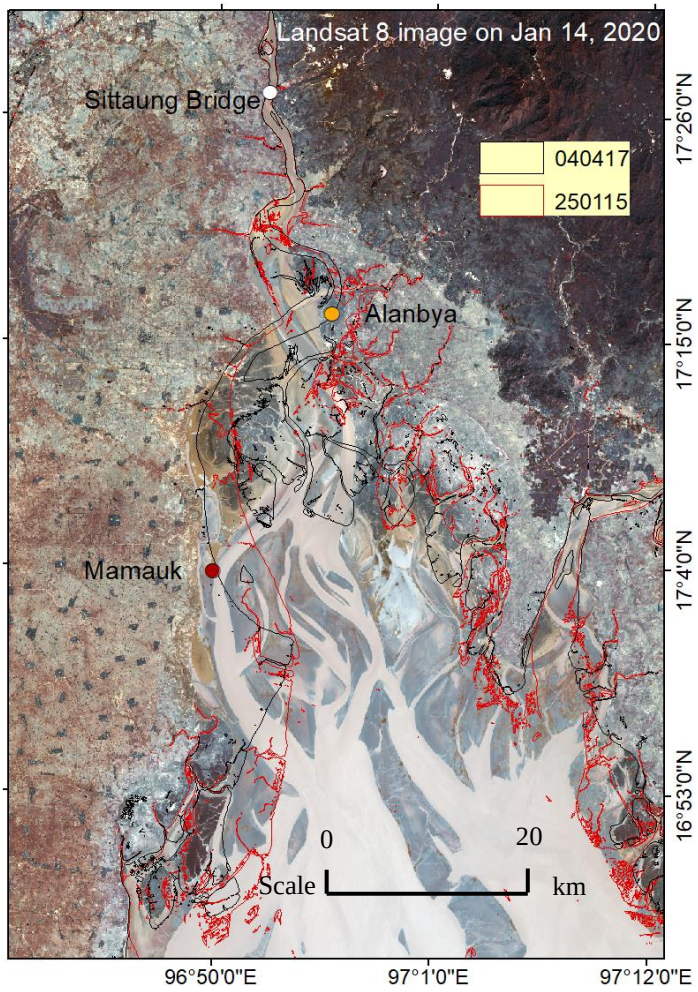

Figure 2. Landsat 8 image on 14th January, 2020. Bank lines on January, 2015 and April, 2017 are superimposed on the recent satellite image.

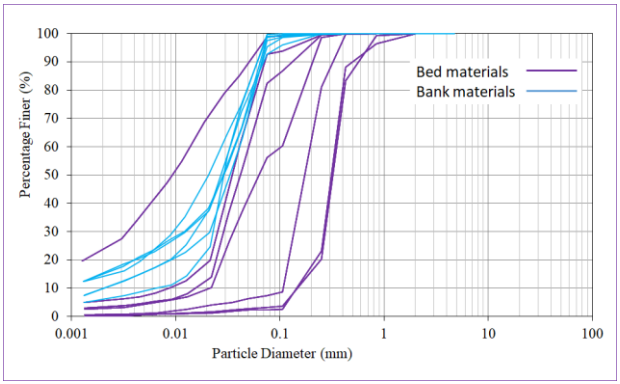

Figure 3. Grain size distribution analysis of bed and bank materials. Bed materials were collected in the upstream of Sittaung Bridge on February, 2019.

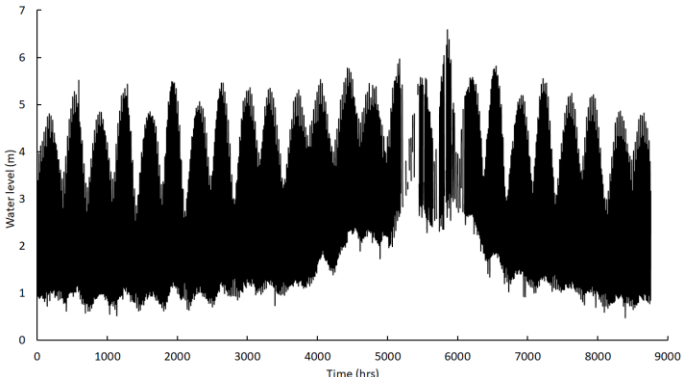

Figure 4. Observed water level by UHSLC at Mawlamyine in 2019.

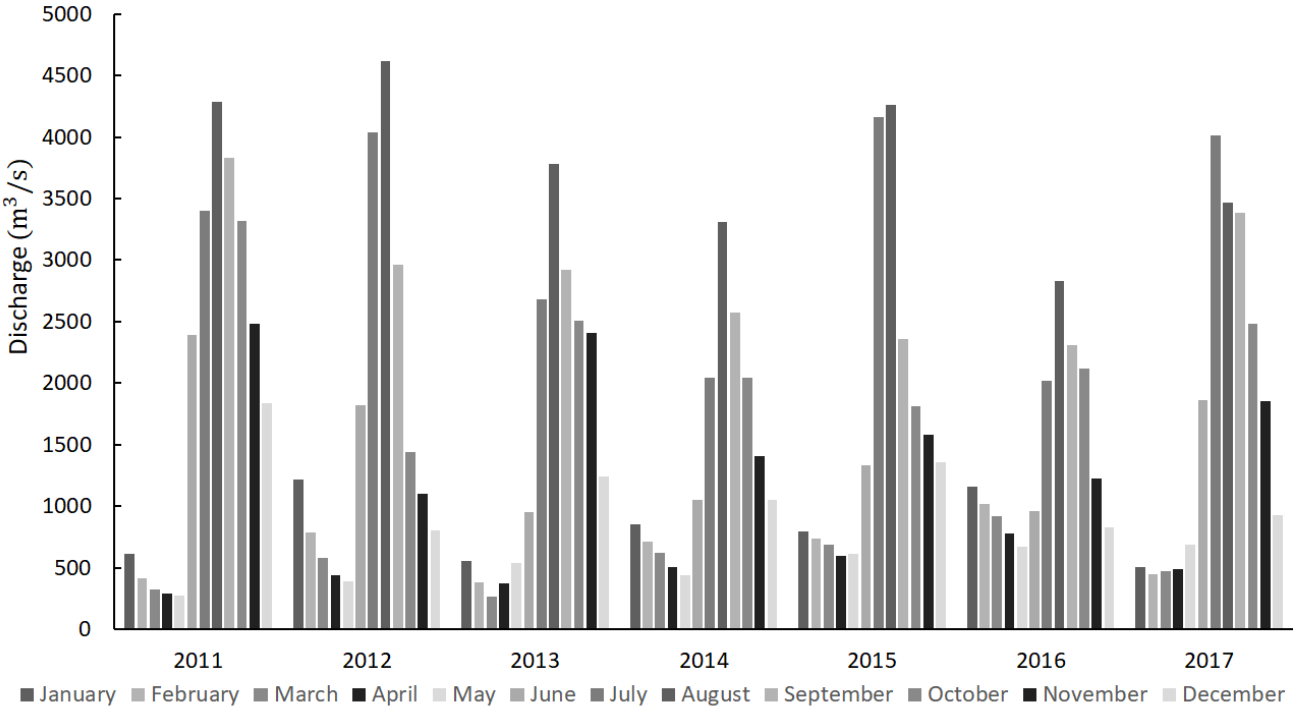

Figure 5. Discharge measured at Madauk in these years.

University of Hawaii for water level at Mawlamyine in 2019. It is seen from the tidal information that in January, February and March, maximum tidal range reaches more than 4 m. Flow discharge is observed at Madauk located 50 km upstream of the Sittaung Bridge. According to data in latest 10 years shown in Figure 5, average flood discharge is about 3000 m^3/s during monsoon from July to September and low flow discharge ranges 300 to 500 m^3/s in dry period.

3. GOVERNING EQUATIONS FOR TIDAL CURRENTS AND BED EVOLUTION

Tidal currents and associated morphological processes are described by means of depth integrated two dimensional governing equations which are composed of mass and momentum conservation equations for the flow body and also mass conservation equations for bed sediment as well as the suspended sediment. The equations are as follows.

$$\frac{\partial h}{\partial t}+\frac{\partial uh}{\partial x}+\frac{\partial vh}{\partial y}=0 \tag{1}$$

$$\frac{\partial uh}{\partial t}+\frac{\partial uuh}{\partial x}+\frac{\partial uvh}{\partial y}=-gh\frac{\partial(h+z_b)}{\partial x}-\frac{\tau_x}{\rho}+\frac{1}{\rho}\left(\frac{\partial h\tau_{xx}}{\partial x}+\frac{\partial h\tau_{yx}}{\partial y}\right) \tag{2}$$

$$\frac{\partial vh}{\partial t}+\frac{\partial vuh}{\partial x}+\frac{\partial vvh}{\partial y}=-gh\frac{\partial(h+z_b)}{\partial y}-\frac{\tau_y}{\rho}+\frac{1}{\rho}\left(\frac{\partial h\tau_{yy}}{\partial y}+\frac{\partial h\tau_{xy}}{\partial x}\right) \tag{3}$$

$$\frac{\partial z_b}{\partial t}+\frac{1}{c_s}\left(\frac{\partial q_{bx}}{\partial x}+\frac{\partial q_{by}}{\partial y}+E-D\right)=0 \tag{4}$$

$$\frac{\partial ch}{\partial t}+\frac{\partial cuh}{\partial x}+\frac{\partial cvh}{\partial y}=\frac{\partial}{\partial x}\left(h\varepsilon_x\frac{\partial c}{\partial x}\right)+\frac{\partial}{\partial y}\left(h\varepsilon_y\frac{\partial c}{\partial y}\right)+E-D \tag{5}$$

In which h is the flow depth, t is the time, u and v are the x and y components of depth-averaged velocity, g is gravitational acceleration, z_b is the bed elevation, ρ is the mass density of water, τ_{xx}, τ_{yy}, τ_{xy} and τ_{yx} are the depth-averaged Reynolds stresses, τ_x and τ_y are the x and y components of the bed shear stress, ε_x and ε_y are the x and y components of turbulent diffusion co-efficient, c is the depth-averaged sediment concentration, c_s is the sediment concentration of bed surface layer, q_{bx} and q_{by} are the x and y components of bed load transport rate, E and D are the erosion and deposition rates of the suspended sediment respectively. The bed shear stress and depth averaged Reynolds stress are evaluated by conventional tools. Formulas for bed load rate and erosion rate, which are proposed in order to treat bed sediment composed of clay-silt particles (Harada et al., 2019), are employed. Those formulas are as follows.

$$\frac{q_b}{u_*h_s}=\frac{1}{6}c_s\frac{u_*h_s}{\nu_s} \tag{6}$$

$$E=W_ec_s \tag{7}$$

In which u_* is the shear velocity, h_s is the thickness of bed load layer, c_s is the sediment concentration of bed surface layer, ν_s is the kinematic viscosity of bed load layer and W_e is the entrainment velocity at the interface between the bed load layer and the upper flow layer. The thickness of bed load layer can be evaluated using an apparent internal friction angle (Harada

et al. 2019). The entrainment velocity is evaluated using the result obtained from density stratified flow (Ashida & Egshira, 1980).

$$\frac{W_e}{\sqrt{u^2+v^2}} = \frac{K}{R_{i*}} \tag{8}$$

In which K is the empirical constant specified as $K = 0.0015$, R_{i*} is overall Richardson number defined as

$$R_{i*} = \frac{\frac{\Delta\rho}{\rho} gh}{u^2+v^2}; \left(\frac{\Delta\rho}{\rho} = \left(\frac{\sigma}{\rho} - 1\right) c_s\right) \tag{9}$$

In which σ is the mass density of sediment particles and ρ is the mass density of ambient fluid. The deposition rate is given by means of fall velocity.

$$D = w_0 c \tag{10}$$

4. COMPUTATION DOMAIN AND CALCULATION CONDITIONS

4.1 Computation domain for tidal currents

The entire Gulf of Martaban is considered as computation domain referring to the estuary shape in 2019 shown in Figure 6 to investigate the occurrences of tidal bore and associated tidal currents. Occurrence of tidal bore is tested by computing temporal change of computed water surface elevation at Station 1 and the validity of the present computation is tested by comparing the computed and observed tidal waves at Station 2.

The upstream condition is specified by the flow discharge of 1000 m^3/s. The specified discharge is larger than those in the dry season illustrated in Figure 5. As the discharge measuring site is 50 km upstream of Sittaung Bridge, drainage area of the site is much less. So, for computing, we need to add some more discharge to those observed in the dry season. The water surface elevation is specified at the downstream boundary as a sine curve with amplitude of 2.3 m and a period of 12 hrs. Flat bed with very mild longitudinal slope of 0.0001 is employed as initial bed surface elevation.

General grid system is employed for computation where Δx is around 200 m along the north-south direction and Δy varies from 30 m at Sittaung bridge location to around 1200 m at the end of Gulf of Martaban. However at the observation location of propagation of tidal bore i.e. near the Mamauk village site, Δx and Δy are about 200 m respectively. Computation time step is 1 s and flow pattern is surveyed every 5 s to catch discontinuous change of water level representing tidal bore. Moreover, to find formative condition of tidal bore, tidal motion of different amplitudes with 0.2 m, 0.5 m, 0.8 m, 0.9 m, 1 m, 1.2 m, 1.5 m and 2.3 m and a period of 12 hrs are employed as downstream boundary conditions.

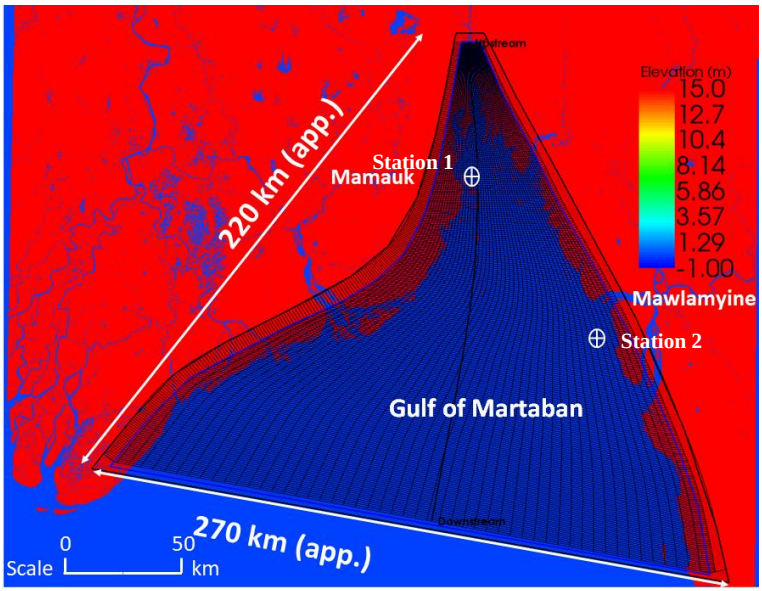

Figure 6. Computation domain to investigate occurrences of tidal bores and associated currents.

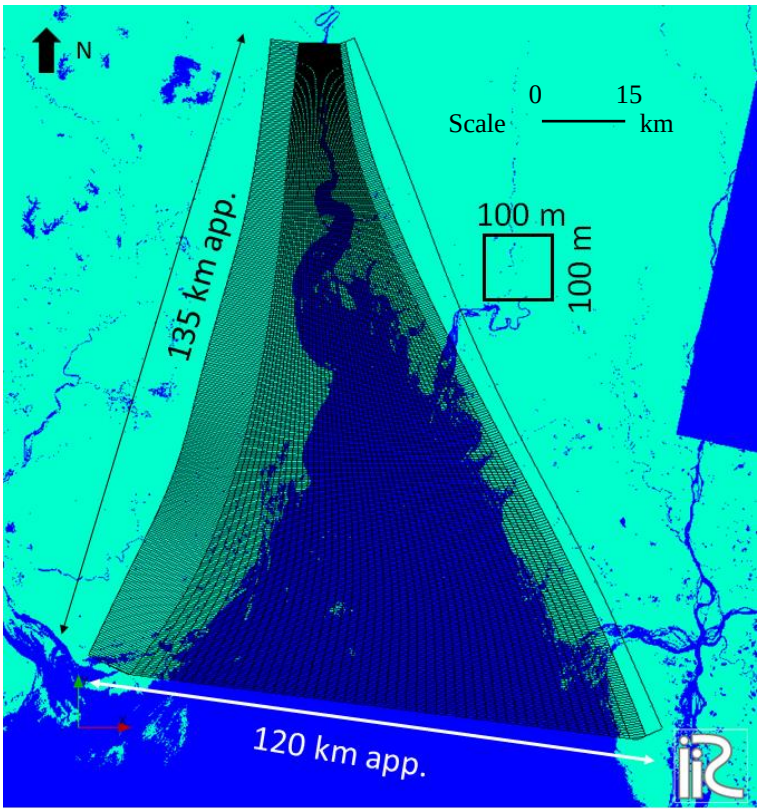

Figure 7. Computation domain to investigate sediment transport processes and bed evolution.

4.2 Domain for bed evolution

Figure 7 shows the computation domain to investigate sediment transport processes and corresponding channel changes. The domain, which is reduced for computational time saving, is determined based on the shape of the estuary

during the dry season in January, 2017. The computation domain is approximately 135 km long from the upstream boundary which is set around 20 km upstream from the Sittaung Bridge and approximately 120 km wide at the downstream boundary. Reference grain size of bed material is specified as 0.03 mm based on the field investigation results. Average flood discharge of 3000 m^3/s is employed as upstream boundary condition according to the discharge data at Madauk. The water surface elevation is specified at the downstream boundary as a sine curve with the amplitude of 2 m and the period of 12 hrs according to data provided by University of Hawaii Sea Level Centre. Initial bed surface is flat and inclines longitudinally in slope of 0.0001. General grid system is employed where Δx is 100 m along the north-south direction and Δy varies from 40 m at the upstream boundary to around 550 m at the downstream boundary. Computation time step is 0.2 s. An equilibrium sediment concentration of suspended sediment is employed at upstream boundary. At the downstream boundary, gradient of suspended sediment concentration is set to be zero. c_s is specified as 0.2 (Ahmed et al., 2019). The International River Interface Cooperative (iRIC) software by Nelson et al. (2016) is employed to conduct present numerical simulation.

5. COMPUTED RESULTS AND DISCUSSION

5.1 Tidal currents

Numerical simulation is conducted based on the conditions mentioned in the earlier chapter. Figure 8(a), (b) and (c) show the water surface elevation employed at the downstream boundary, the numerically simulated results of water surface elevations at Station 1 & Station 2 and the computed water surface elevation at Station 2 as well as observed water level information collected from the University of Hawaii Sea Level Centre website. Results illustrated in Figure 8 (b) and (c) show that the tidal motion specified at the downstream boundary is

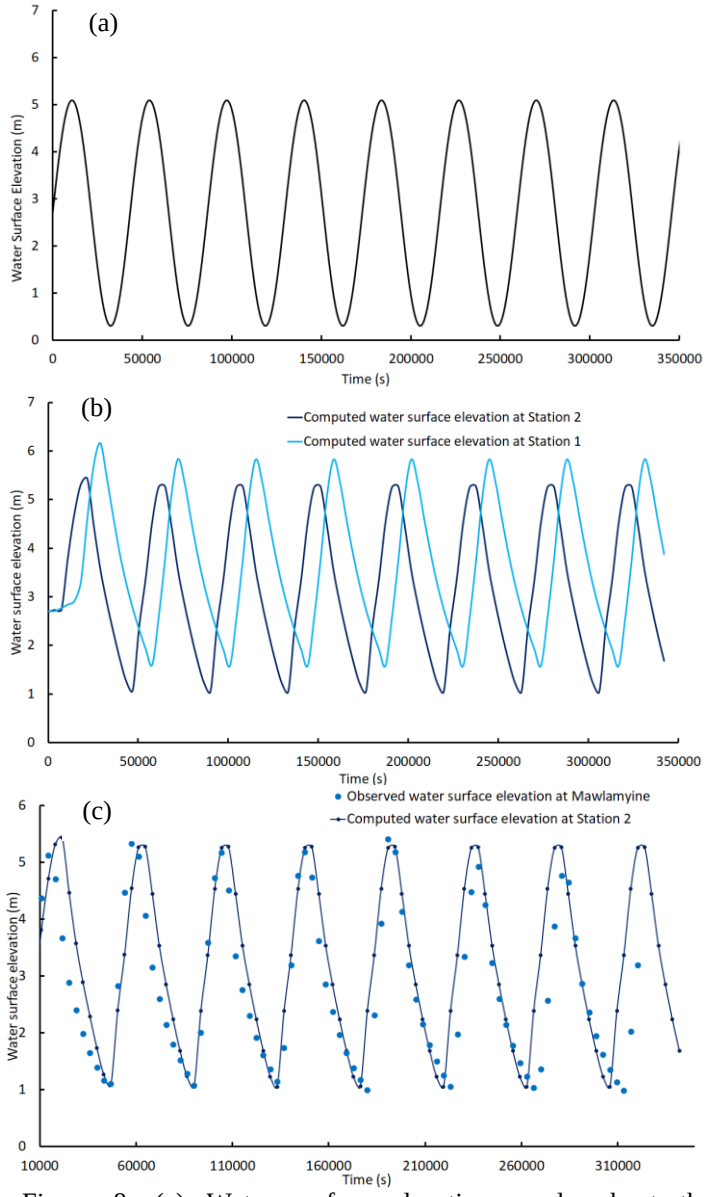

Figure 8. (a) Water surface elevation employed at the downstream boundary of computation domain, (b) computed water surface elevations at Stations 1 & 2 and (c) comparison of computed and observed water surface elevations at Station 2 and at Mawlamyine.

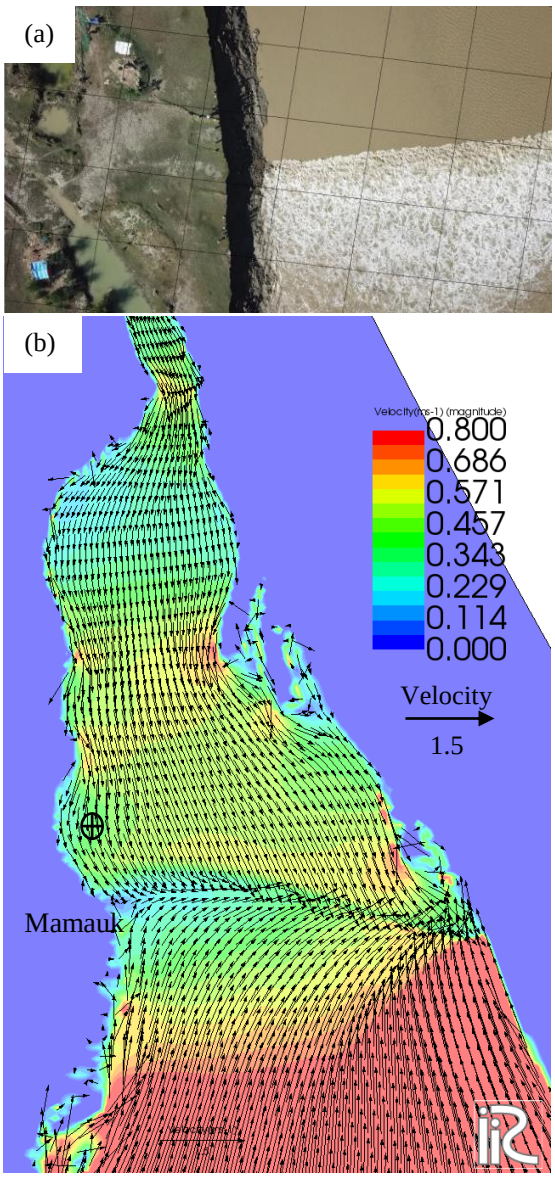

Figure 9. (a) Tidal bore front captured using Unmanned Aerial Vehicle (UAV) during the field observation and (b) computed velocity field reproducing a tidal bore front near Mamauk.

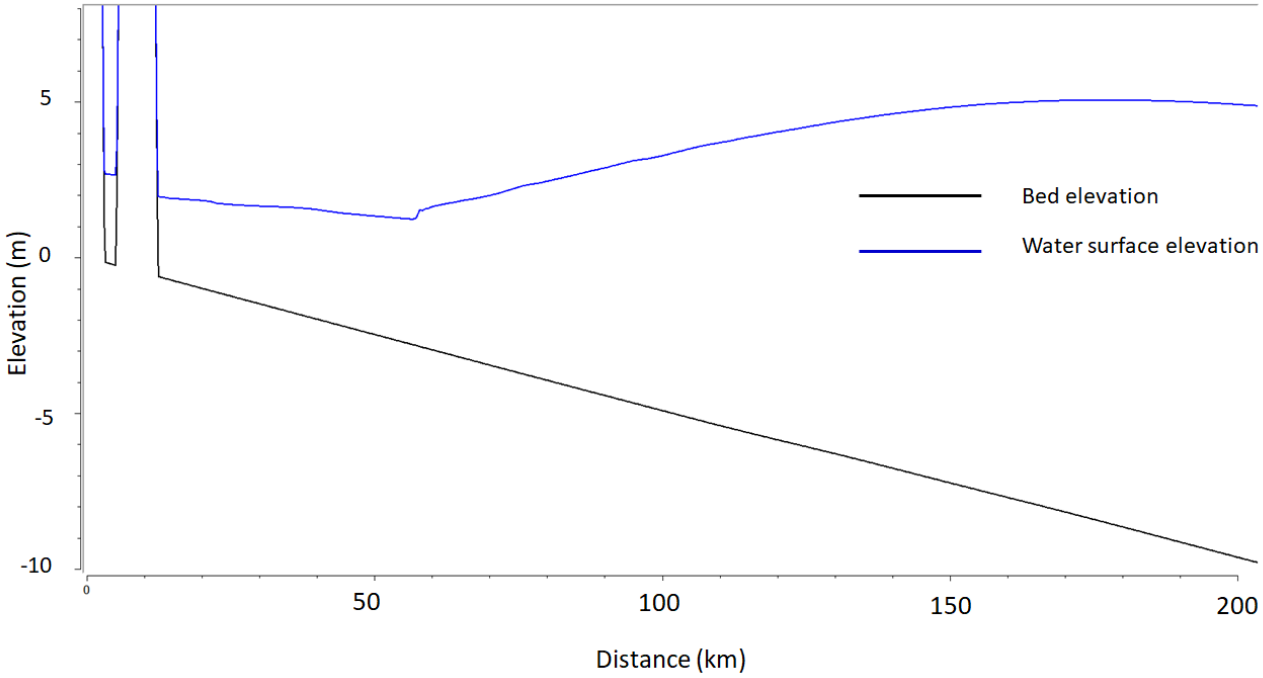

Figure 10. Computed water surface elevation along the computation domain where discontinuous change in water surface elevation is observed when tide propagates upstream.

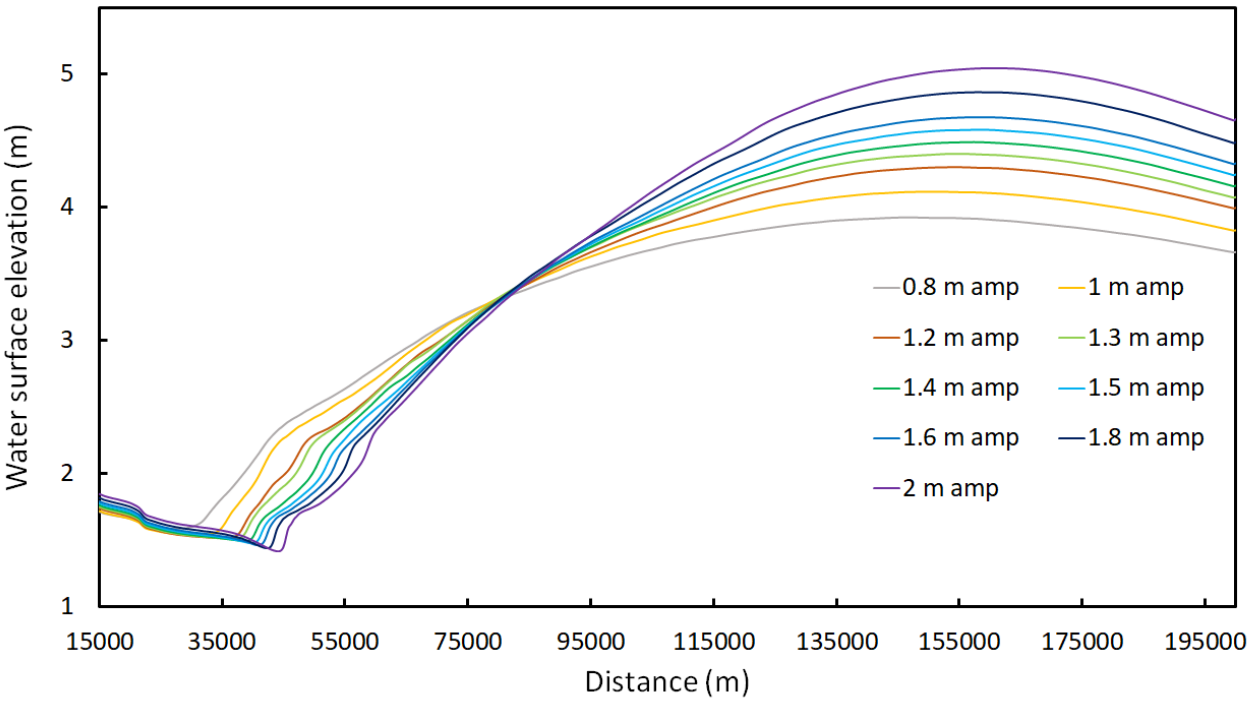

Figure 11. Longitudinal profiles of computed water surface elevations based on downstream boundary water surface elevations of different amplitudes.

deformed and the deformed tidal motion is reproduced well at Station 2. Figure 9(a) and (b) show a still picture of propagation of tidal bore near Mamauk taken using an Unmanned Aerial Vehicle (UAV) during the field observation on February, 2019 and the computed velocity field that reproduces tidal bore near Mamauk. Two opposing velocity vectors in two consecutive grids represent propagation of tidal bore followed by strong tidal currents which are illustrated as red coloured fringe in Figure 9(b). Figure 10 shows a computed water surface profile. The profile realizes a discontinuous change forming at the tidal bore front followed by high tides. Figure 11 shows water surface profiles which are computed using tidal motions of different amplitudes employed at the downstream boundary. The results realizes that tidal bores may be reproduced in all cases of the tidal amplitudes from 0.8 m to 2.0 m although their front heights might be different. In order to discuss occurrence conditions of tidal bores, we need to investigate their decaying process.

5.2 Sand bar evolution

Figure 12(a), (b), (c) and (d) shows the numerical results on developing process of sand bars and stream channel pattern obtained from the computations of 20, 40, 70 and 90 days. It is recognized that the computed stream channel pattern and the bed morphology are created well in the estuary. Formation of sand bars and scour areas show similarity with the erosion and deposition prone areas on the satellite images. Figure 13(a) and (b) show the computed bed evolution after 90 days on the estuary shape of February, 2019 and the Landsat 8 satellite image of 26th April, 2019. The created morphology shows good agreement with the satellite image that the blue circled area in the satellite image is a big sand bar and deposition zone that is created well in the computed bed elevation. In addition, stream channel pattern shows similar tendency exhibited in the satellite image. Computed results suggest that the proposed methodology can successfully reproduce the bed morphology and stream channel pattern. We may need data on longitudinal, lateral bed profile to test the validity of the present numerical model. However, bed elevation in the estuary can't be measured due to very shallow morphology and rapid movement of sand bars in low tide and tidal bore and strong tidal currents during high tide.

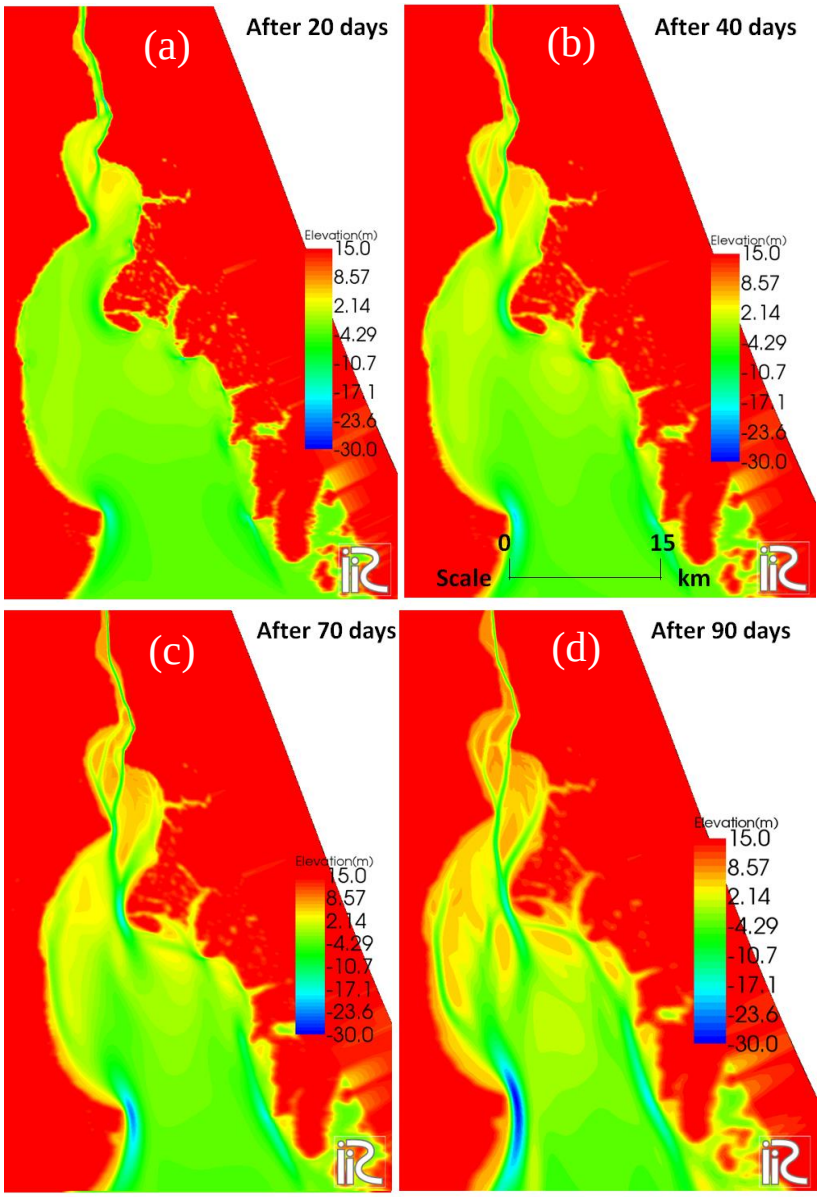

Figure 12. Developing process of sand bars and stream channel pattern on the January, 2017 estuary shape.

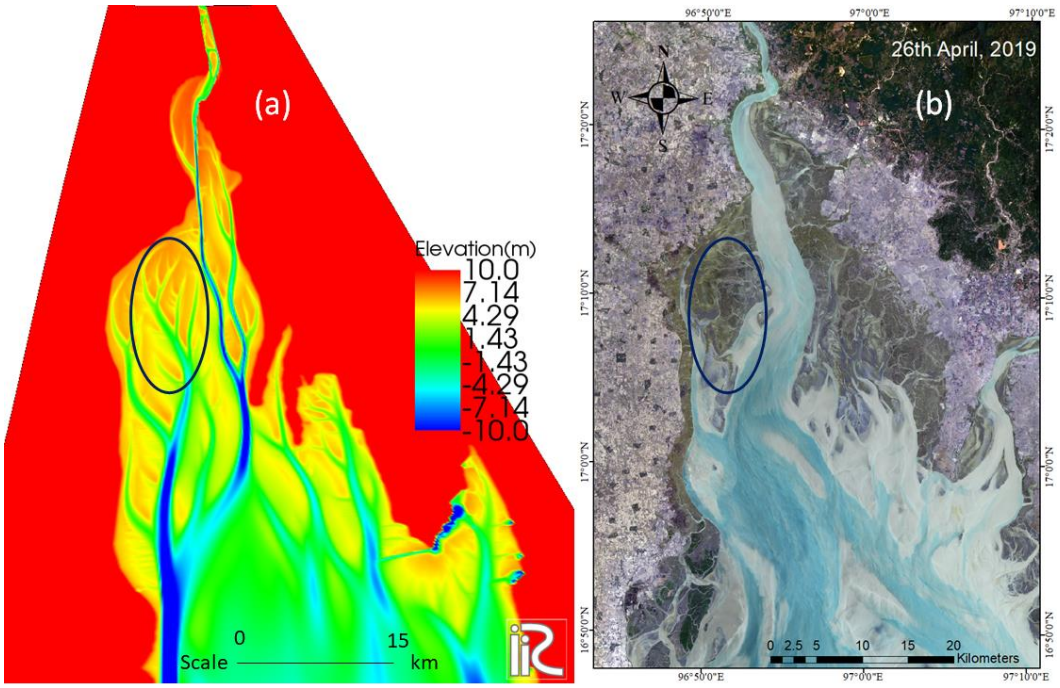

Figure 13. (a) Computed bed evolution after 90 days on the shape of the estuary on February, 2019 and (b) Landsat 8 satellite image on April 26, 2019.

6. CONCLUSIONS

Present study discusses tidal currents and associated sediment transport processes based on numerical results as well as on satellite image data including field surveyed data in Sittaung River estuary where the estuary bed and banks are composed mainly of silt-clay particles. Results are summarized as follows:

(1) A new method to evaluate very fine sediment transport is combined with a conventional two dimensional depth averaged flow model. (2) The new method reproduces tidal bores and associated tidal currents, temporal, spatial changes of bed morphology such as braided channel pattern and deformation of sand bars.

However, there are many problems to be studied; the applicability of the proposed method, occurrence condition of tidal bores, side bank erosion, etc.

ACKNOWLEDGMENTS

The Authors are grateful to the staff members joined in the survey activities during the field investigation in Myanmar. Staff members of Directorate of Water Resources and Improvement of River Systems (DWIR) in Myanmar helped the Authors continuously for field surveys and data collections. The Authors are grateful to them.

REFERENCES

Ahmed, T.S., Egashira, S., Harada, D., Yorozuya, A.: Sediment transportation and sand bar deformation owing to tidal currents in Sittaung river estuary, Myanmar, *Journal of Japan Society of Civil Engineers, Ser. B1 (Hydraulic Engineering)*, Vol. 75, No. 2, I_1027-I_1032, 2019.

Ashida, K., Egashira, S.: Studies on the Structures of Density Stratified flows, *Bulletin of the Disaster Prevention Research Institute*, 29(4), pp. 165-198, 1980.

Harada, D., Egashira, S., Ahmed, T.S., Katayama, N.: Erosion Rate of Bed Sediment by means of Entrainment Velocity, *Journal of Japan Society of Civil Engineers*, Ser. B1 (Hydraulic Engineering), Volume 75, Issue 4 (published).

Lanzoni, S., Seminara, G.: Long-term evolution and morphodynamic equilibrium of tidal channels, *Journal of Geophysical Research*, Vol. 107, No. C1, 3001, 10.1029/2000JC000468, 2002.

Lesser, G.R., Roelvink, J.A., van Kester, J.A.T.M., Stelling, G.S.: Development and validation of a three-dimensional morphological model, *Coastal Engineering*, 51 (2004) 883-915.

Nelson, J.M., Shimizu, Y., Abe, T., Asahi, K., Gamou, M., Inoue, T., Iwasaki, T., Kakinuma, T., Kawamura, S., Kimura, I., Kyuka, T., Mcdonald, R.R., Nabi, M., Nakatsugawa, M., Simoes, F.R., Takebayashi, H., Watanabe, Y.: The International River Interface Co-operative: Public domain flow and morpho-dynamics software for education and applications. *Advances in Water Resources*, Vol. 93, pp. 62-74, 2016.

Robinson, R.A.J., Bird, M.I., Oo, N.W., Hoey, T.B., Aye, M.M., Higgitt, D.L., Lu, X.X., Tun, T., Win, S.L.: The Irrawaddy river sediment flux to the Indian Ocean: the original nineteenth century data revisited, *Journal of Geology*, 115 (2007), 629-640.

Shimozono, T., Tajima, Y., Akamatsu, S., Matsuba, Y.,Kawasaki, A.: Large-scale channel migration in the Sittaung river estuary, *Scientific Reports*, (2019), 9:9862.

Ramaswamy, V., Rao, P.S., Rao, K.H., Thwin, S., Rao, N.S., Raiker,V.: Tidal influence on suspended sediment distribution and dispersal in the northern Andaman Sea and Gulf of Martaban, *Marine Geology*, 208 (2004) 33-42.

Yu, Q., Wang, Y., Gao, S., Flemming, B.: Modeling the formation of a sand bar within a large funnel-shaped, tide-dominated estuary: Qiantangjiang Estuary, China, *Marine Geology*, 299-302 (2012) 63-76.